ISBN: 978-3-95450-208-0 doi:10.18429/JACoW-IPAC2019-MOPMP026

HE-LHC OPTICS DESIGN OPTIONS

J. Keintzel*[1], M. Crouch , M. Hofer[1], T. Risselada, R. Tomás, F. Zimmermann
CERN, Geneva, Switzerland
L. van Riesen-Haupt, John Adams Institute, University of Oxford, Oxford, UK
[1]also at Vienna University of Technology, Vienna, Austria

Abstract

The High Energy Large Hadron Collider (HE-LHC), a possible successor of the High Luminosity Large Hadron Collider (HL-LHC) aims at reaching a centre-of-mass energy of about 27 TeV using basically the same 16 T dipoles as for the hadron-hadron Future Circular Collider FCC-hh. Designing the HE-LHC results in a trade off between energy reach, beam stay clear as well as geometry offset with respect to the LHC. In order to best meet the requirements, various arc cell and dispersion suppressor options have been generated and analysed, before concluding on two baseline options, which are presented in this paper. Merits of each design are highlighted and possible solutions for beam stay clear minima are presented.

INTRODUCTION

Various possible successors of the Large Hadron Collider (LHC) are studied within the framework of the Future Circular Collider (FCC) study [1]. Within this framework, effort is put into the design of the High Energy LHC (HE-LHC), a synchrotron with 26.7 km circumference, which aims at reaching 27 TeV centre-of-mass (c.o.m.) energy using of the same 16 T dipoles the hadron-hadron FCC (FCC-hh). Therefore, this accelerator is planned to achieve twice the c.o.m. energy of the LHC, while being installed in the tunnel which hosted already the LHC and the Large Electron Positron collider (LEP). On one hand, installing the HE-LHC in the existing tunnel has the advantage of less civil engineering work, while, on the other hand, it imposes strong geometry constraints on the layout. As a result, the functionalities of the eight Interaction Regions (IRs) [2] remain unchanged from LHC. The main experiments are therefore located in IR1 and IR5, Beam 1 and Beam 2 are injected in IR2 and IR8, respectively, the RF insertion is located in IR4, momentum collimation and betatron collimation insertions located in IR3 and IR7, respectively, as well as the beam dump of both beams in IR6. In addition, in the tunnel of the Super Proton Synchrotron (SPS) which provides currently 450 GeV beam energy, a new fast ramping superconducting synchrotron (scSPS) with an extraction beam energy above 1 TeV could be installed to serve as injector for the HE-LHC.

BASELINE OPTIONS

Before concluding on the two baseline designs described in this paper, different arc FODO cell and dispersion suppressor options have been generated and matched using MAD-X [3] and analysed. In order to generate a tremendous number of lattice configurations, a tool named ALGEA (Automatic Lattice GEneration Application) was developed, which is continually being improved. Detailed results can be found in [4, 5].

Arc Cells

The cell length is chosen to keep the bending radius in the arcs similar to LHC. With a filling factor of 81 % achieved by a 18×90 (18 LHC-like FODO cells per arc with 90° phase advance per cell) design, a c.o.m. energy of 27 TeV can be reached, whereas a 23×90 design provides a c.o.m. energy of roughly 26 TeV, assuming 16 T dipoles. At injection energy however, the 23×90 profits from the smaller beam size and dispersion and has, therefore, a larger beam stay clear (BSC) compared to the 18×90 design. The most promising configurations are a 18×90 and a 23×90 design, where the latest parameters are summarised in Table 1.

Table 1: Parameters of the HE-LHC Design Options

Parameter	Unit	18×90	23×90
Cell Length	m	137.19	106.90
Dipoles per Cell	–	8	6
Dipole Length	m	13.92	13.73
Filling Factor	%	81	77
Quadrupole Length	m	2.8	3.3
Quadrupole Strength	T/m	335	352
β_{min}/β_{max} in Cell	m	41/230	32/177
D_{min}/D_{max} in Cell	m	1.7/3.6	1.1/2.2
c.o.m. Energy at 16 T	TeV	27.24	25.83
Field for 27 TeV	T	15.8	16.7
BSC at 450 GeV	σ	7.51	8.78

Every dipole (MB) is equipped with a sextupole spool piece corrector (MCS). In addition, an octupole and decapole corrector (MCO, MCD) are attached to every second dipole. The short straight section (SSS), the bending-free space between a dipole and a quadrupole (MQ), contains an orbit corrector (MCB), a sextupole (MS), a Beam Position Monitor (BPM) and a trim quadrupole (MQT). It has to be noticed, that eight MQTs per arc are exchanged against four octupoles and four skew quadrupoles. Moreover, four MS per arc are replaced by skew sextupoles. Further details can be found in [6]. In Fig. 1 the two different cell layouts are shown.

* jacqueline.keintzel@cern.ch

ISBN: 978-3-95450-208-0 doi:10.18429/JACoW-IPAC2019-MOPMP026

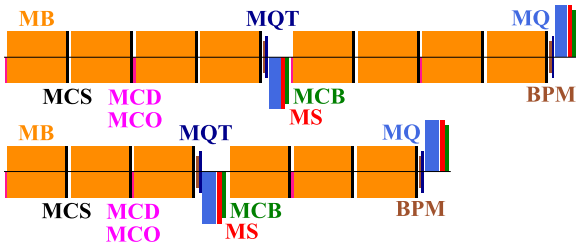

Figure 1: Arc-cell layout of the 18×90 (upper) and 23×90 (lower) design.

Dispersion Suppressor

The integrated dispersion suppressor (DS) is split into an irregular and a regular part, where layout of the latter is identical to the first arc FODO cell. The irregular part, containing eight dipoles and three 4.5 m long individually-powered quadrupoles (MQ8 - MQ10), is separated by the arc cell by a drift space of approximately 13 m. This layout combines commonly used dispersion suppression techniques [7]: reduced number of dipoles per DS cell, compared to an arc cell, resulting in one long drift space, as well as individually powered quadrupoles (MQ8 - MQ10) or trim quadrupoles (MQT11 - MQT13). Compared to previous designs [8], more effort is put into finding the most suitable length and position of the irregular DS part, in order to reduce the transverse offset to LEP geometry. A schematic plot of the irregular part of the DS for the two lattice options, right from the IRs, is given in Fig. 2.

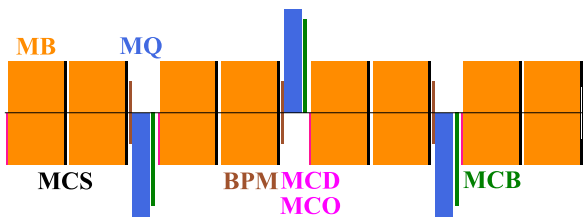

Figure 2: Irregular part of the DS, right of the IR, for the baseline options, integrated in all IRs.

It has to be noticed that in the LHC the DS neighbouring IR3 and IR7 are different due to smaller available space in the tunnel for individual power converters [2]. MQ8 to MQ10 are hence powered identical to the arc MQs, while the desired optics is achieved by additional individually-powered trim quadrupoles, requiring smaller power converters. This additional constraint has not been applied to the HE-LHC.

Moreover, studies assuming a conservative quench limit of 5 mW/cm^3 [9], predict the need of additional collimators (TCLD) in the DS sections neighbouring IR1, IR3, IR5 and IR7 for ion operation [10] and proper collimation [11]. These TCLDs will increase the length of the DS, which can lead to an increased geometry offset with respect to LHC and LEP. Alternative collimation approaches include crystal collimators [12] or additional orbit bumps for ion operation in IR1 and IR5. Further work studying the necessity and the lattice integration of possible collimation options will be needed before concluding on a DS design.

Lattices

Several specially-designed IRs have currently been integrated in the lattice (IR1 and IR5 [13], IR4 [14], IR6 [15], IR3 and IR7 [16]). IR2 and IR8 remain unchanged with respect to LHC [2]. To match the fractional part of the working point at collision energy, (0.31, 0.32), the tune is compensated by quadrupoles in IR4 and MQs in Arcs 23, 34, 67 and 78, leading to a small phase advance change in the respective arcs, while preserving 90° per cell in the arcs neighbouring the main experiments [17]. At injection energy, the MQTs are used to trim the tune to the LHC working point (0.28, 0.31).

As already stated above, a major constraint on the HE-LHC design is the tunnel geometry. The transverse offset of the average beam path from LEP must therefore not exceed significantly the offset of LHC to LEP, which is about 6.5 cm peak-to-peak. Figure 3 shows the transverse offset of the average beam of LHC and the HE-LHC baseline lattices with respect to LEP. The peak-to-peak difference is about 8 cm in case of the 18×90 and about 3 cm for the 23×90 design, where in all lattices the maximum offset is located in the DS, as seen in Fig. 3. Both baseline designs are, therefore, assumed to fit in the existing tunnel.

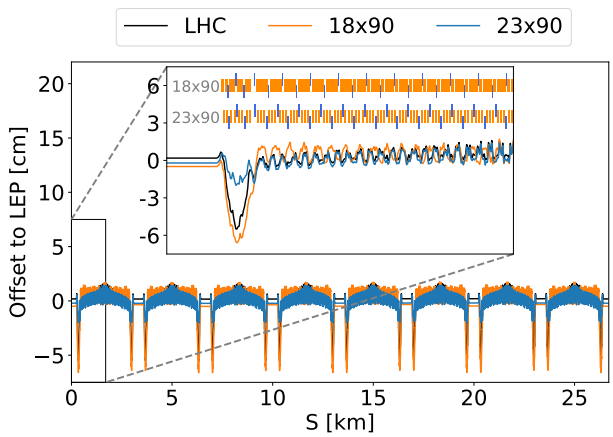

Figure 3: Geometry offset of HE-LHC options and LHC with respect to LEP.

BEAM STAY CLEAR

The BSC describes the available space for the beam in the beam screen in units of the standard deviation σ and can be approximated through [18]

$$BSC = \frac{L - t - k_\beta D \delta_p}{k_\beta \sigma}, \quad (1)$$

where L and t are the beam screen dimensions and tolerances, respectively, D the dispersion function, $k_\beta = \sqrt{1 + \Delta\beta/\beta}$ the β-beating factor and $\delta_p = \Delta p/p$ the relative momentum offset. A minimum value of $10\,\sigma$ over the ring is required

ISBN: 978-3-95450-208-0 doi:10.18429/JACoW-IPAC2019-MOPMP026

to ensure enough space for proper collimator settings [19]. The BSC computation is performed with MAD-X, respecting more parameters than used in the approximation given in Eq. (1), where the FCC-hh beam screen, presented in 2018 [20], is used. At 450 GeV, the current injection energy provided by the SPS, none of the baseline designs fulfills this target. In the following, proposals to increase the BSC are discussed. Moreover, complementary studies regarding the dynamic aperture (DA) are summarised in [21].

Probably the most obvious solution is a beam screen enlargement. Applying a scaling factor of 20 % or 12 % to the beam screen, results in sufficient BSC in case of the 18×90 or the 23×90 designs, respectively. A larger beam screen for constant outer magnet dimension could imply a reduced magnetic field, i.e. lower than 16 T.

As the beam size decreases with increasing energy, another possibility to enlarge the BSC is injecting at higher energy. To reach 10 σ 800 GeV is required for the 18×90 design, whereas about 600 GeV is sufficient for the 23×90 one. Replacing half of the magnets in the SPS with superconducting ones, would result in an achievable energy of about 600 GeV, which was already proposed in 1972 [22].

A stronger focusing effect and therefore a smaller beam size can be achieved using combined-function dipoles (CFD). The magnetic field expansion reads [23]

$$B_y + iB_x = B_{\text{ref}} \sum_{n=1}^{\infty} (b_n + ia_n) \left(\frac{x+iy}{R_{\text{ref}}} \right)^{n-1} , \qquad (2)$$

where the terms a and b indicate skew and normal components, respectively, and B_{ref} the magnetic field at the reference radius R_{ref}. CFD have an additional quadrupole component, corresponding to b_2 in Eq. (2). To reach 10 σ BSC, an additional b_2 component in the dipoles of 450×10^{-4} are sufficient for both designs. It has to be noticed, however, that the feasibility of two different magnet types, i.e. providing $+450 \times 10^{-4}$ at the inner aperture simultaneously to -450×10^{-4} at the outer one and vice versa, is assumed. The best combination of these additional focusing fields is schematically shown in Fig. 4.

The current baseline foresees horizontal (μ_x) and vertical (μ_y) phase advances of 90° per cell in both transverse planes, which was found to be beneficial for corrections of chromatic errors [17]. Nevertheless, phase advances impact the BSC and therefore a phase advance scan from 72° to 108° has been performed as shown in Fig. 5. Special phase advances

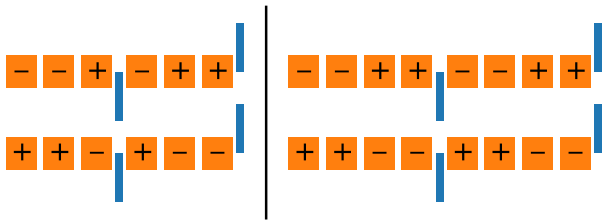

Figure 4: Combined-function dipole configuration for the 23 (right) and 18 (left) cells designs.

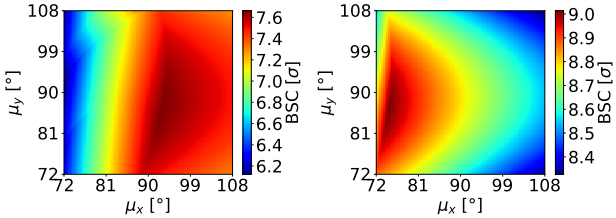

(a) 18×90 (b) 23×90

Figure 5: Phase dependence of the BSC.

$\mu_{x,y} = 2\pi(n_{x,y}/N_c)$ which fulfill [24]

$$k_1 n_x + k_2 n_y = kN_c \text{ with } k_1 \neq k_2 , \qquad (3)$$

where $k_1, k_2, k, n_x, n_y \in \mathbb{N}$ and N_c the number of cells (number of FODO cells plus 2 irregular DS cells) per arc, generate resonance-free lattices (RFL). Although RFL maximise the DA, resonance cancelling phase advances are found which also improve the BSC slightly. The exact values can be found in Table 2 together with the nominal values, and the phase advances, which result in the largest BSC.

Table 2: Horizontal (μ_x) and vertical (μ_y) phase advances and the resulting BSC for the baseline (BL), Resonance Free Lattices (RFL) and the BSC maximization (MAX) at 450 GeV.

	18 Cells			**23 Cells**		
	μ_x [°]	μ_y [°]	BSC [σ]	μ_x [°]	μ_y [°]	BSC [σ]
BL	90.0	90.0	7.51	90.0	90.0	8.78
RFL	90.0	72.0	7.53	72.0	86.0	8.82
MAX	90.5	86.7	7.66	74.5	86.8	9.01

CONCLUSION

Two baseline designs are presented, where the major constraint, the installation of the ring in the tunnel, is fulfilled, as the geometry offset to LEP is 3 cm for the 23×90 design, and 8 cm for the 18×90 one, where the latter exceeds the offset of LHC to LEP only by 1.5 cm. Nevertheless, designs regarding collimation approaches are currently explored to identify the most suitable collimation setting and the effect on the geometry. The great advantage of the 18×90 design is the c.o.m. energy of 27 TeV, compared to about 26 TeV for 23×90 design. At injection energy, the 23×90 has smaller beam sizes and therefore larger BSC. At 450 GeV, the beam energy provided by the SPS, however, none of the options reaches 10 σ BSC. Promising solutions to meet this target are proposed, namely injecting at higher energies, demanding an upgrade of the SPS, enlarging the beam screen, using combined function dipoles or varying the phase advance. To conclude, the work presented in this paper highlights some key challenges in designing the HE-LHC lattice. Solutions have already been found regarding the geometry. Future work will finalise the lattice and optics of the HE-LHC.

ISBN: 978-3-95450-208-0 doi:10.18429/JACoW-IPAC2019-MOPMP026

REFERENCES

[1] FCC study, https://fcc.web.cern.ch/.

[2] O.S. Brüning *et al.*, "LHC Design Report", CERN Yellow Reports: Monographs, 2004.

[3] MAD-X, http://mad.web.cern.ch/mad/.

[4] J. Keintzel, "Arc Cell Options for the HE-LHC", CERN-ACC-2018-0020, 2018.

[5] J. Keintzel, "Optics Design and Performance Aspects of the HE-LHC", Master Thesis, CERN-THESIS-2018-177, presented Sep. 2018.

[6] Future Circular Collider Study. Volume 4: The High Energy LHC (HE-LHC) Conceptual Design Report, preprint edited by F. Zimmermann et al. CERN accelerator reports, CERN-ACC-2018-0059, Geneva, December 2018. Submitted to Eur. Phys. J. ST.

[7] B. Holzer, "Beam Optics and Lattice Design for Particle Accelerators", arXiv:1303.6514, 2013.

[8] M. Hofer *et al.*, "Integrated Full HE-LHC Optics and Its Performance", in *Proc. 9th Int. Particle Accelerator Conf. (IPAC'18)*, Vancouver, Canada, Apr.-May 2018, pp. 348–351. doi:10.18429/JACoW-IPAC2018-MOPMK002

[9] Future Circular Collider Study. Volume 3: The Hadron Collider (FCC-hh) Conceptual Design Report, preprint edited by M. Benedikt et al. CERN accelerator reports, CERN-ACC-2018-0058, Geneva, December 2018. Submitted to Eur. Phys. J. ST.

[10] J. Jowett, Private Communication, 2018.

[11] M. Crouch, Private Communication, 2018.

[12] D. Mirarchi, "Crystal Collimation System: Concept and Layouts", presented at the HL-LHC Crystal Collimation Day, CERN, Geneva, 2018. https://indico.cern.ch/event/752062/contributions/3114826/

[13] L. van Riesen-Haupt *et al.*, "Experimental Interaction Region Optics for the High Energy LHC", in *Proc. 9th Int. Particle Accelerator Conf. (IPAC'18)*, Vancouver, Canada, Apr.-May 2018, pp. 360–363. doi:10.18429/JACoW-IPAC2018-MOPMK006

[14] L. van Riesen-Haupt *et al.*, "Optics for RF Acceleration Section for the High Energy Large Hadron Collider", in *Proc. 9th Int. Particle Accelerator Conf. (IPAC'18)*, Vancouver, Canada, Apr.-May 2018, pp. 345–347. doi:10.18429/JACoW-IPAC2018-MOPMK001

[15] W. Bartmann *et al.*, "Injection and Dump Systems for a 13.5 TeV Hadron Synchrotron HE-LHC", in *Proc. 9th Int. Particle Accelerator Conf. (IPAC'18)*, Vancouver, Canada, Apr.-May 2018, pp. 858–861. doi:10.18429/JACoW-IPAC2018-TUPAF060

[16] T. Risselada, Private Communication, 2019.

[17] S. Fartoukh, "The Right Optics Concept for the Right Dimension of the High Luminosity LHC Project", ICFA Beam Dyn.Newsl. **71** 116-135, CERN-ACC-2016-0085, 2016.

[18] J. Jeanneret and T. Risselada, "Geometrical Aperture in LHC at Injection", LHC-ProjectNote-66, 1996.

[19] R. Bruce, Private Communication, 2018.

[20] R. Kersevan, "New Beam Screen Design Proposal", Presented at the FCC-hh General Design Meeting, CERN, Geneva, 2018. https://indico.cern.ch/event/715957/contributions/2943304/

[21] M. Hofer, M. Giovannozzi, J. Keintzel, R. Tomas, F. Zimmermann, and L. van Riesen-Haupt, "Dynamic Aperture at Injection for the HE-LHC", presented at the 10th Int. Particle Accelerator Conf. (IPAC'19), Melbourne, Australia, May 2019, paper MOPMP023, this conference.

[22] CERN, "The 300 GeV Programme", CERN-1050, 1972.

[23] O. Brüning and S. Fartoukh, "Field Quality Specification for the LHC Main Dipole Magnets", CERN-LHC-Project-Report-501, 2001.

[24] A. Verdier, "Resonance Free Lattices for Alternating Gradient Machines", CERN-SL-99-018-AP, 1999.